JOURNAL OF AIRCRAFT
Vol. 41, No. 5, September–October 2004

Understanding Ducted-Rotor Antitorque and Directional Control Characteristics Part I: Steady-State Simulation

Emre Alpman* and Lyle N. Long†
The Pennsylvania State University, University Park, Pennsylvania 16802
and
Bruce D. Kothmann‡
Boeing Defense and Space Group, Philadelphia, Pennsylvania 19142-0858

Despite decades of very successful yaw-control and antitorque applications, the aerodynamics of ducted rotors in low-power, near-edgewise flow conditions are not well understood. Motivated by phenomena discovered during the development of the RAH-66 Comanche's directional-axis control laws, a research program was initiated to use computational fluid dynamics to improve the understanding of the dynamic relationship between ducted-rotor thrust and applied collective pitch, especially when the rotor is operating in near-edgewise flight conditions. This paper is a presentation of the results of this study. Numerical solutions of the inviscid Euler equations were obtained for the flow over the Comanche fuselage with a uniform actuator disk and blade element models for the FANTAIL™; the main rotor is excluded in this study. The solutions were obtained by running the modified PUMA2 (Parallel Unstructured Maritime Aerodynamics) computational-fluid-dynamics code with an unstructured grid with 2.8 million tetrahedral cells. Excellent correlation between the calculations and a variety of static test data are presented and discussed. Subsequent efforts will examine the important aspects of the dynamics of the thrust response, and allow further comparisons with flight-test data.

Nomenclature

A_{disk}	=	fan disk area
a	=	lift-curve slope
Cp	=	pressure coefficient
C_l	=	lift coefficient
C_T	=	thrust coefficient
c	=	fan blade chord
L	=	total length of the helicopter
l	=	blade section lift
M_∞	=	freestream Mach number
N_b	=	number of fan blades
R	=	blade radius
R_{cb}	=	radius of the centerbody
r	=	radial blade station
T	=	period of one blade passage
T_{fan}	=	fan thrust
t	=	time
V_N	=	normal velocity
V_T	=	tangential velocity
V_∞	=	freestream velocity
x	=	streamwise helicopter station
α	=	local blade angle of attack
$\acute{\alpha}$	=	helicopter angle of attack
Δp	=	pressure jump
θ	=	local blade pitch angle
θ_0	=	collective pitch angle
$\theta_{.75}$	=	blade pitch angle at $\frac{3}{4}$ radius
θ_1	=	linear blade twist
ρ	=	fluid density
σ	=	fan solidity
ϕ	=	inflow angle
ψ	=	azimuth angle
Ω	=	blade rotation speed

Received 9 July 2003; revision received 4 September 2003; accepted for publication 5 September 2003.

*Graduate Research Assistant, 229 Hammond Building; exa152@psu.edu.

†Professor of Aerospace Engineering, 229 Hammond Building; lnl@psu.edu.

‡Flight Mechanics Engineer, P.O. Box 16858 MS P31-31; bruce.d.kothmann@boeing.com.

Introduction

THE ducted rotor offers a number of important benefits over a conventional tail rotor. Safety is notably improved through virtual elimination of tail-rotor strike events. Noise reductions are also dramatic. From a handling-qualities perspective the ducted rotor provides the loads capacity required for very aggressive maneuvers and allows unrivaled sideward flight and sideslip envelopes, among other important advantages.[1–4]

Despite these significant advantages, the ducted tail rotor presents a design challenge in forward flight. To reduce the momentum drag caused by turning the flow through the fan, the nominal operating condition of the ducted rotor is chosen to be near-zero effective mass flux. In contrast to a conventional rotor, for which the large effective mass flux in forward flight tends to linearize thrust response to collective pitch and reduce the importance of inflow dynamics, near-zero effective mass flux through the duct tends to increase the importance of dynamic inflow and render the approximations of conventional momentum theory inadequate.

Experience on the RAH-66 Comanche has shown that, despite substantial improvements in momentum-type models of the steady thrust response of a ducted tail rotor,[5] the dynamics of the total (fan + shroud) thrust response in forward flight are not yet well understood. The unexpected thrust response was first clearly observed shortly after the initial engagement of the core automatic flight-control system mode. Figure 1 shows a sustained, large-amplitude 1-Hz yaw oscillation during a shallow-turning partial-power descent at 80 kn forward speed. (There were no loads or safety issues associated with this oscillation, but it would obviously adversely affect pilot comfort.) These oscillations are not seen in the steady-state results but are only seen in the closed-loop control. Notice that the

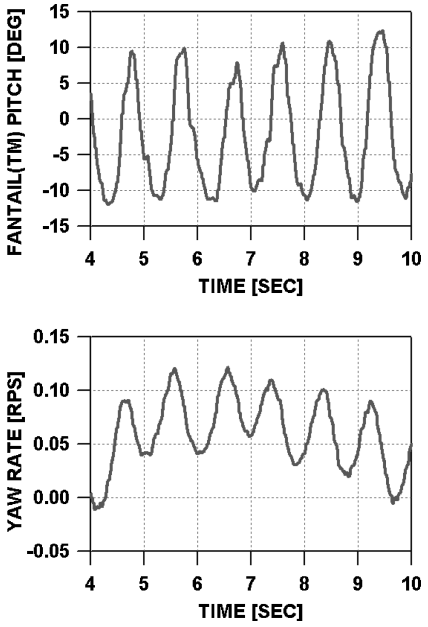

Fig. 1 Sustained 1-Hz directional axis oscillation in shallow turning partial power descent at 80 kn.

average (trim) value of FANTAIL pitch is near zero, where the mass flux through the duct is near zero.

After an exhaustive review of possible causes of the oscillations, including a careful audit of digital processing delays and consideration of stiction in the actuators, among many other factors, the conclusion was reached that there must be a significant apparent delay in the development of thrust in response to collective pitch changes.

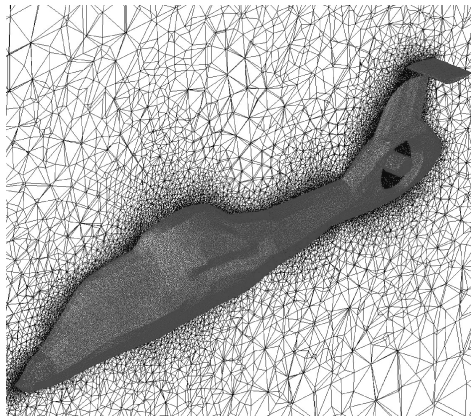

Fig. 4 Computational mesh.

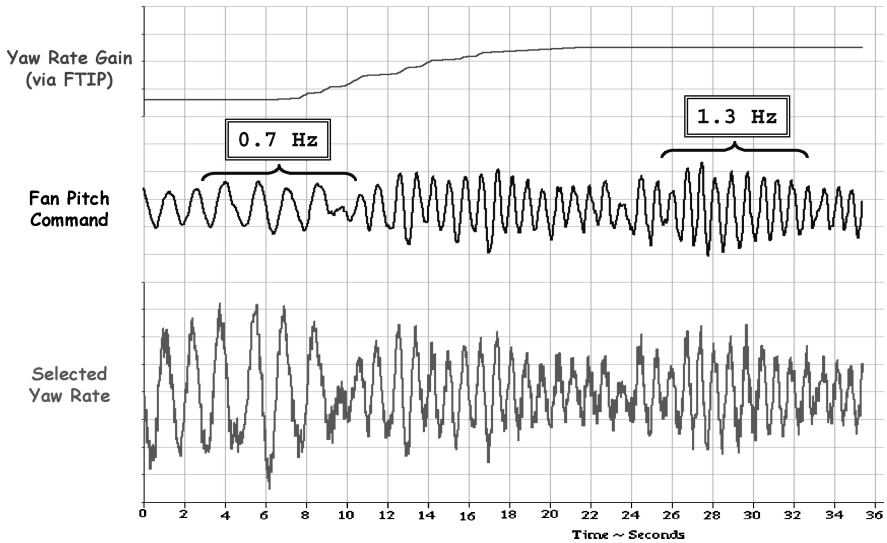

Fig. 2 Effect of yaw rate gain on directional axis-oscillations ($V = 140$ kn). (FTIP: Flight Test Interface Panel.)

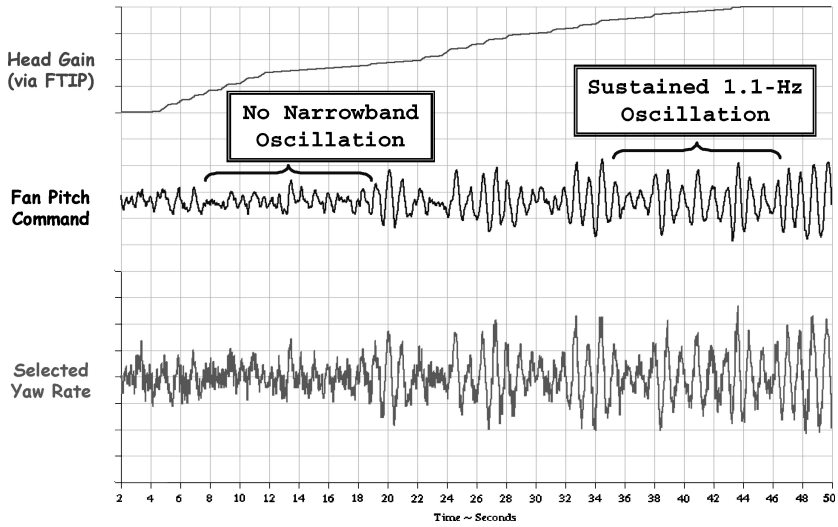

Fig. 3 Effect of heading gain on directional axis-oscillations ($V = 140$ kn). (FTIP: Flight Test Interface Panel.)

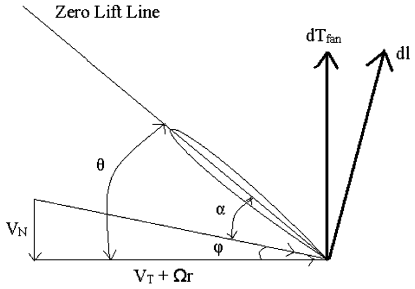

Fig. 5 Blade-element diagram.

One consequence of the delay is that higher yaw rate gain, normally associated with increased damping of the body modes, tends to increase frequency, whereas higher heading gain, normally associated with increased frequency, tends to decrease damping. Figures 2 and 3 show early flight-test data demonstrating the unusual effects of rate and attitude gain changes.

For the Comanche combinations of changes in directional-axis feedback with modifications in the empennage configuration were sufficient to satisfy the ADS-33 analytical requirements and also to ensure mission effectiveness.[6,7] The current effort was undertaken to improve the understanding of the aeromechanics of ducted tail rotors in forward flight with the hope of enabling further improvements in this very successful technology.

Methodology

This paper analyzes the flowfield around the fuselage of an RAH-66 Comanche helicopter with and without the fan-in-fin operating. Computational fluid dynamics (CFD) is used because it allows a more complete mathematical model to make quantitative predictions of complex flows dominated by nonlinear effects.[8] Potential flow theory,[9,10] Euler equations,[11] and Navier–Stokes equations[9,12–14] have been used in the literature to define flowfields around helicopters. Each of these methods has an associated computational cost and benefit.[13] In this study the flowfield is assumed to be inviscid, and the predictions are made using Euler equations. The antitorque system of the helicopter, which is a ducted fan called the FANTAIL (Ref. 15), is modeled using an actuator disk, in which the fan-in-fin is assumed to be a rotor with zero thickness.[16] Although the fan blades could be modeled in more detail, we are trying to develop a method that requires minimal CPU time and can be used in engineering settings. For our purposes here we do not believe that detailed modeling of the tip-gap region or blade swirl is critical. We are also assuming that the timescales of the blades are much smaller than the timescale of the outer flow. Two different methods are followed to introduce the effects of the FANTAIL to the overall flowfield. In the first method the fan thrust is set as an input by applying a uniform pressure jump across the actuator disk. On the other hand, in the second method the blade collective pitch angle is set as an input, and the corresponding fan thrust and aerodynamic forces are computed. Computations are performed for hover, forward-flight, and sideward-flight conditions. The governing equations are solved on an unstructured grid with 2.8 million tetrahedral cells, which can be seen in Fig. 4. This number of cells is adequate to achieve good agreement with wind-tunnel test data and is also a case that can be run in a reasonable time on a Beowulf cluster. For example, hover cases require approximately 38 hours of computer time on four nodes, each consisting of dual 800-MHz Pentium III processors with 1024 MB RAM and dual 100 Mbps fast Ethernet cards.

Numerical solutions are performed by first modifying the computer code PUMA2[17–21] (Parallel Unstructured Maritime Aerodynamics), which is written in ANSI C. PUMA2 has been used and validated by Long et al. for numerical solution of numerous problems.[17–29] Parallel processing is applied to reduce the CPU time and memory requirements. The message-passing-interface (MPI)[30] communication standard is used for this purpose, and the code is run on the Beowulf clusters COCOA and COCOA2.[19,21,22]

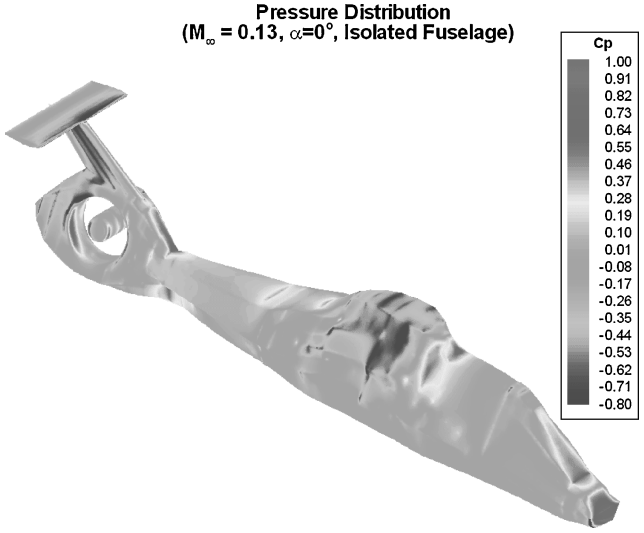

Fig. 6 Pressure distribution over isolated fuselage: $M_\infty = 0.13$, $V_\infty = 85.9$ kn, and $\alpha = 0$ deg.

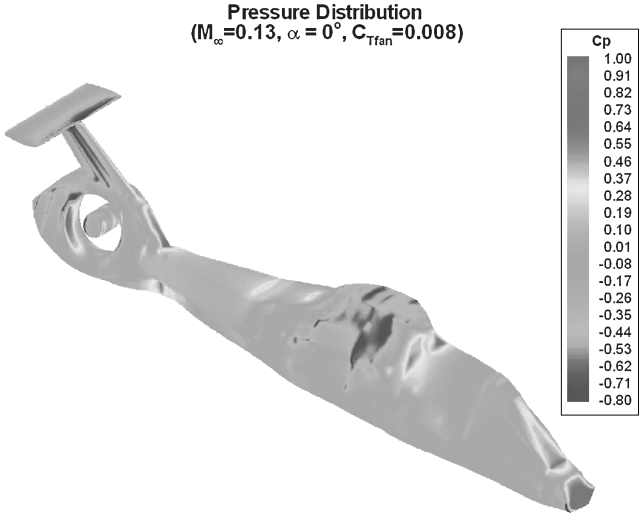

Fig. 7 Pressure distribution over fuselage: $M_\infty = 0.13$, $V_\infty = 85.9$ kn, $\alpha = 0$ deg, and $C_{\text{Tfan}} = 0.008$.

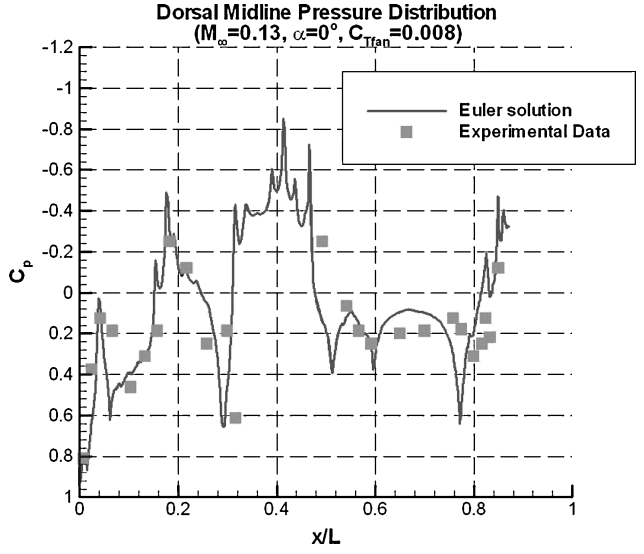

Fig. 8 Comparison of computed dorsal midline pressure distribution with experiment: $M_\infty = 0.13$, $V_\infty = 85.9$ kn, $\alpha = 0$ deg, and $C_{\text{Tfan}} = 0.008$.

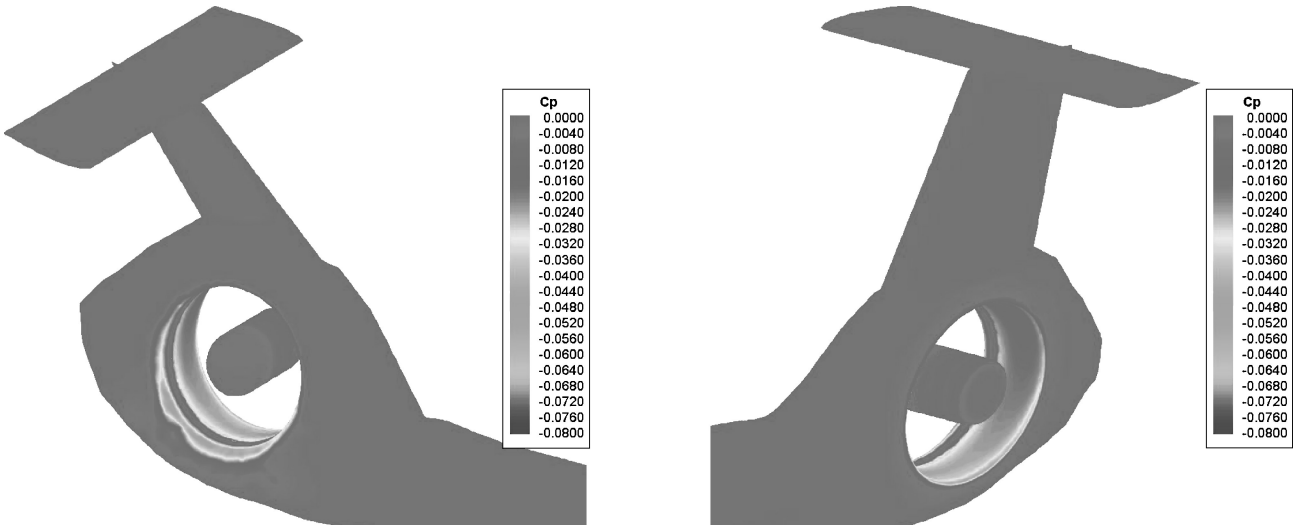

Fig. 9 *Cp* contours in the vicinity of FANTAIL: hover, starboard, and port views, with $\theta_{.75} = -10$ deg.

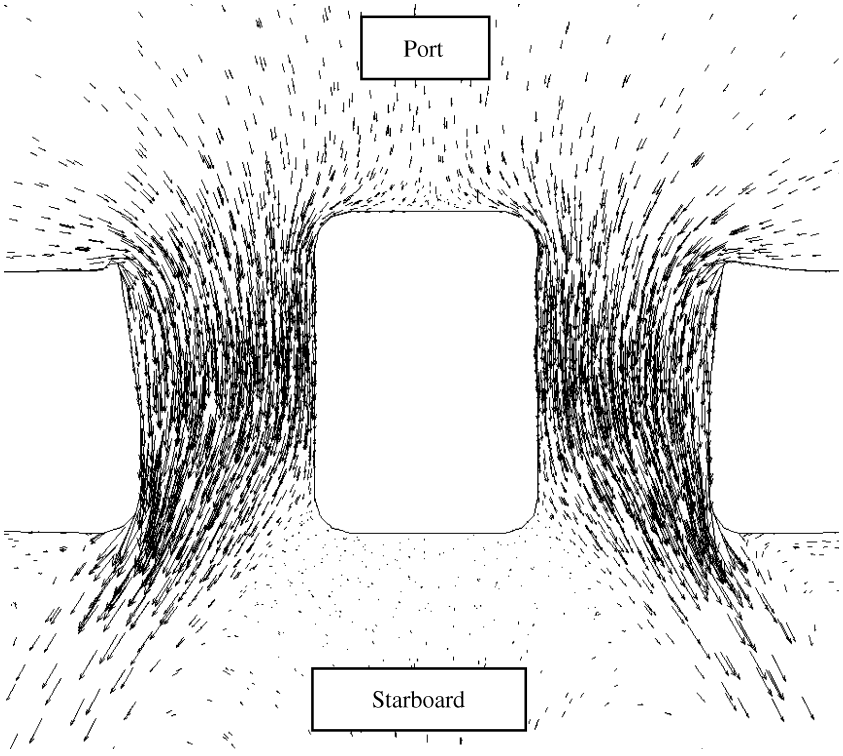

Fig. 10 Velocity vectors in the vicinity of FANTAIL: hover, with $\theta_{.75} = -10$ deg. (Net thrust is towards port side.)

FANTAIL Modeling

The FANTAIL is modeled as an actuator disk with zero thickness. Its effects are introduced into the flow as boundary conditions in which the pressure undergoes a discontinuity while the other flow parameters remain continuous. Uniform-momentum theory and blade-element theory are used.

Uniform-Momentum Theory

In this approach fan thrust is set as an input, and the uniform pressure jump is computed as follows:

$$\Delta p = T_{\text{fan}}/A_{\text{disk}} \tag{1}$$

where

$$A_{\text{disk}} = \pi\left(R^2 - R_{\text{cb}}^2\right) \tag{2}$$

Blade-Element Theory

In this approach the collective pitch angle of the blades is set as an input, and the corresponding fan thrust is computed by using blade-element theory, which relates the local lift on a differential element of the blade to the local velocity and the local blade pitch. The external velocity vector is decomposed into a component normal to the disk $V_N(r, \psi)$ and a component in the plane of the disk $V_T(r, \psi)$. A schematic of the blade element and the corresponding velocities and forces can be seen in Fig. 5. The lift coefficient is assumed to be a unique function of angle of attack by neglecting the Mach-number and Reynolds-number effects. The resulting equations are

$$\alpha(r, \psi) = \theta(r) - \tan^{-1}[V_N/(V_T + \Omega r)] \tag{3}$$

$$l(r, \psi) = \tfrac{1}{2}\rho \cdot c\left[V_N^2 + (V_T + \Omega r)^2\right] \cdot C_l(\alpha) \tag{4}$$

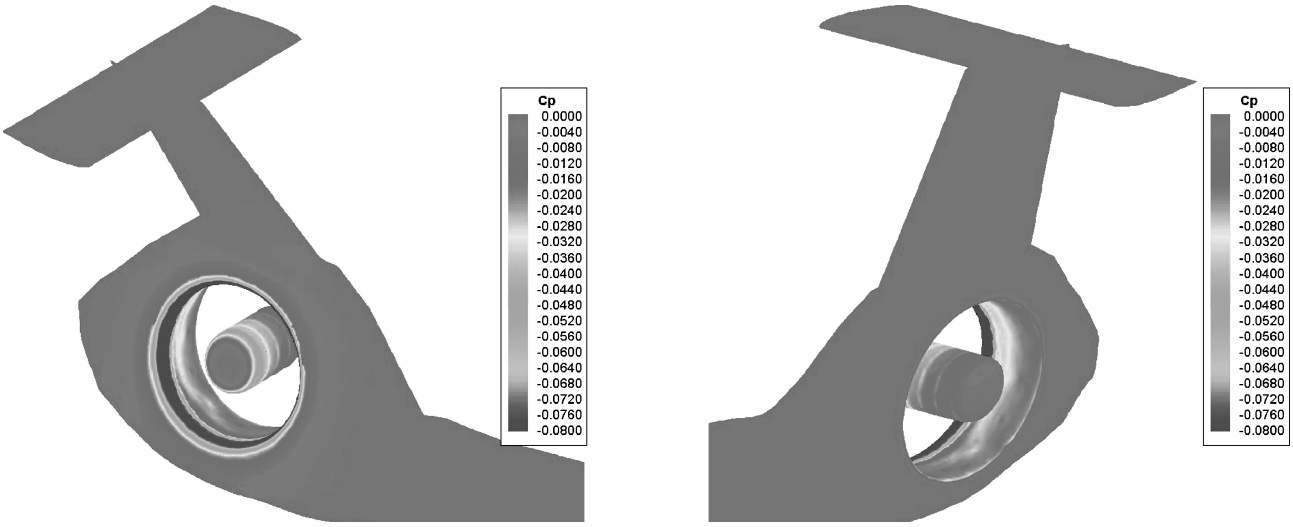

Fig. 11 *Cp* contours in the vicinity of FANTAIL: hover, starboard, and port views, with $\theta_{.75} = 20$ deg.

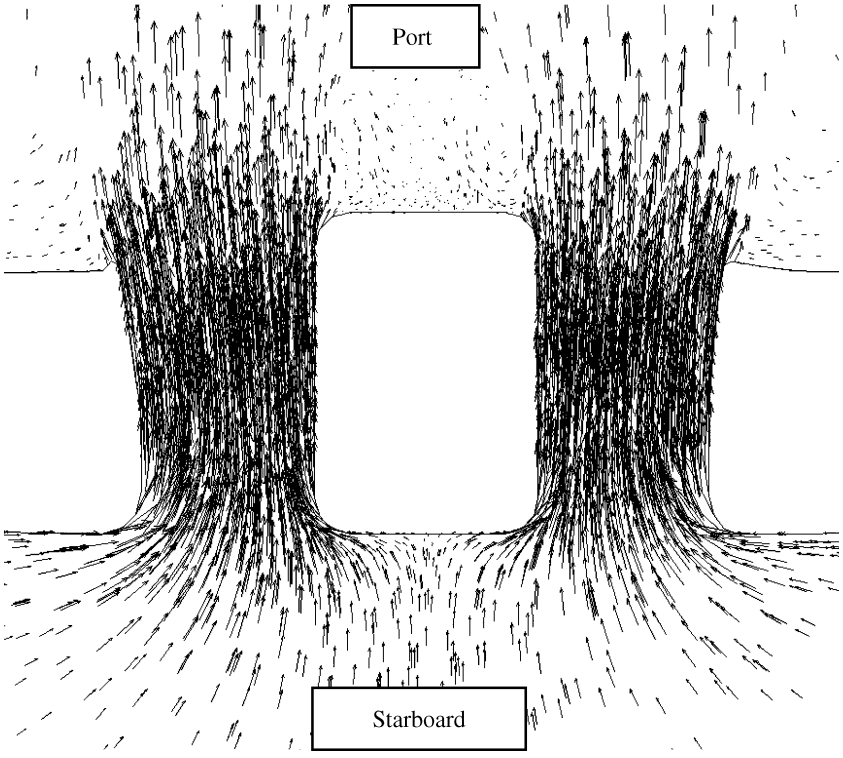

Fig. 12 Velocity vectors in the vicinity of FANTAIL: hover, with $\theta_{.75} = 20$ deg. (Net thrust is towards starboard side.)

An often used approximation is as follows: the linear lift coefficient is given by $C_l = a\alpha$, where $a = 5.73$ 1/rad. The blade pitch is typically approximated by linear twist with respect to the blade pitch at 75% radius. The fan has eight blades; each has a twist angle of 7 deg.

$$\theta(r) = \theta_0 + \theta_1(r/R - 0.75) \tag{5}$$

In the usual simplified theory the blade-element expressions for lift, or more commonly the integrated thrust and moments, are used as inputs to momentum theory to estimate the external flow velocities $V_N(r, \psi)$ and $V_T(r, \psi)$. In the present work momentum theory is replaced by a direct numerical simulation of the external flow. In the present approach the individual blades are not included in the definition of the body boundary. Instead, an actuator disk is used at the nominal plane of the rotor disk to apply pressure-jump boundary conditions to the flow solution. Although the actual pressure jump at a given location on the disk will vary between zero (when no blade is present) and the maximum pressure difference over the blade chord, a useful approximation is to take the average pressure jump during a single blade passage time:

$$\Delta p(r, \psi) = \frac{1}{T}\int_0^T \Delta p_{\text{blade}}(t) \cdot \mathrm{d}t \tag{6}$$

where

$$T = 2\pi / N_b \Omega \tag{7}$$

Now, as just noted, Δp_{blade} will vanish except in those parts of the rotor revolution where some portion of the blade is located at the given station. During these times, the blade is moving with a speed

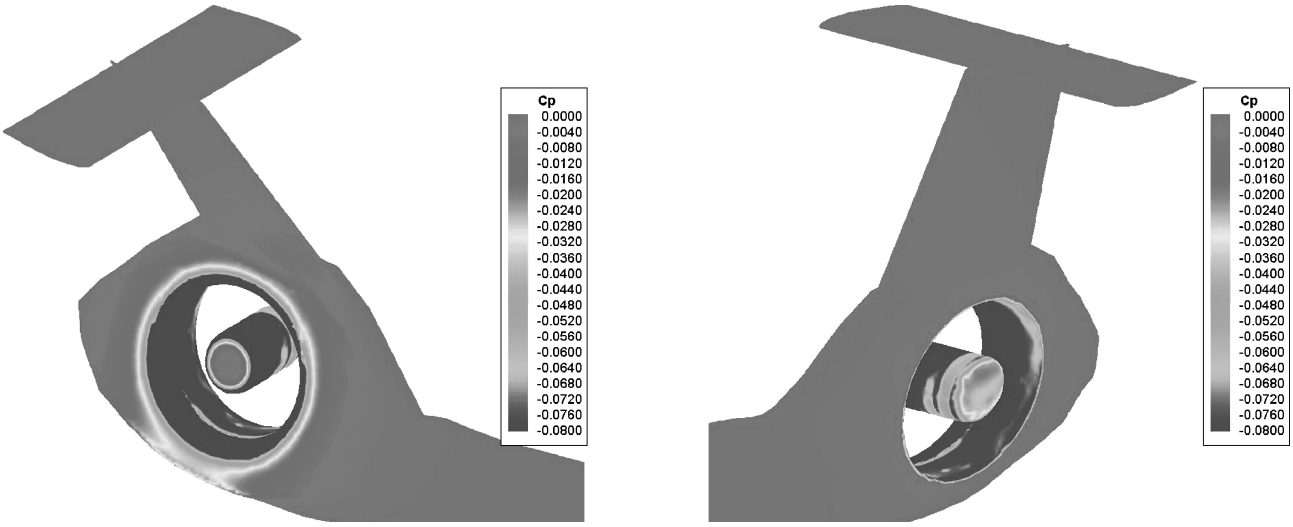

Fig. 13 ***Cp*** **contours in the vicinity of FANTAIL: hover, starboard, and port views, with $\theta_{.75} = 40$ deg.**

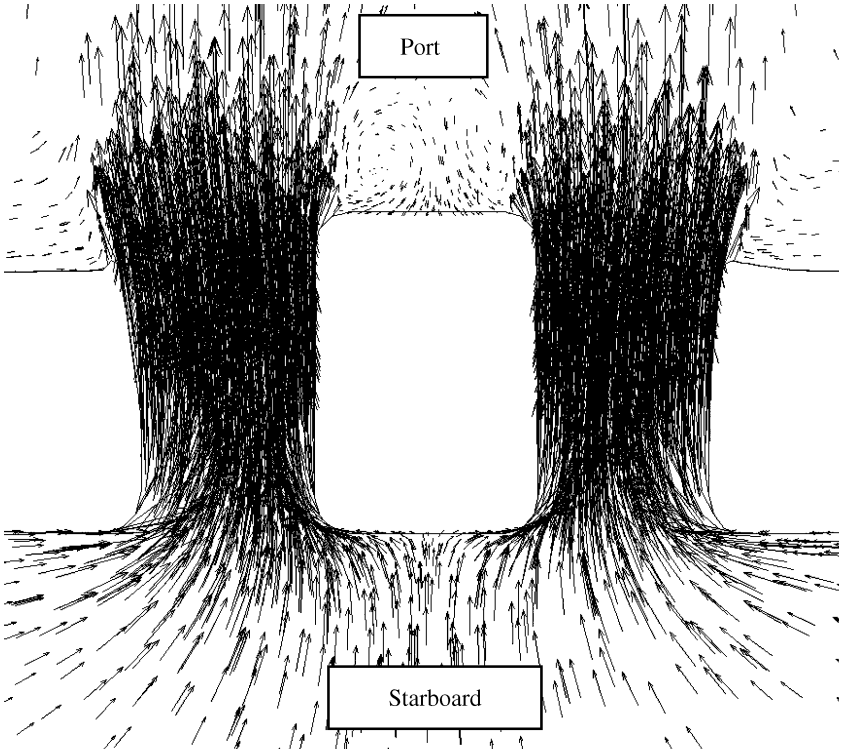

Fig. 14 Velocity vectors in the vicinity of FANTAIL: hover, with $\theta_{.75} = 40$ deg. (Net thrust is towards starboard side.)

of Ωr, so that the variable of integration can be replaced using $\Omega r\, \mathrm{d}t = \mathrm{d}x$:

$$\Delta p(r, \psi) = N_b \frac{\Omega}{2\pi} \int_0^c \Delta p_{\text{blade}}(x) \frac{1}{\Omega r} \cdot \mathrm{d}x \tag{8}$$

Because the integration of blade pressure over the chord is simply the local lift per unit span, the integral can be replaced in favor of the local lift:

$$\Delta p(r, \psi) = N_b \frac{l(r, \psi)}{2\pi \cdot r} \tag{9}$$

Given either a lift coefficient look-up table or linear lift-curve slope and a definition of twist, Eqs. (3–5) and (9) form a complete set of algebraic equations to compute the pressure jump across the disk as a function of computed external flow and the applied collective pitch input θ_0.

Results

Results include flow over an isolated fuselage in forward flight, a FANTAIL modeled with uniform theory in forward flight, and a FANTAIL modeled with blade-element theory in hover, forward and sideward flight cases.

The pressure distribution over the isolated fuselage in forward flight can be seen in Fig. 6. For the solutions coupled with uniform momentum theory, the flow conditions are kept the same as the isolated fuselage case, and the fan thrust coefficient is set to 0.008. Figure 7 shows the surface-pressure distribution, and Fig. 8 shows the comparison of computed and experimental[12] dorsal midline, that is, top of the vehicle, pressure distributions.

Because the fan thrust applied for this case is very small, there is not much difference between isolated fuselage and fan-in-fin operating cases. One can see from Fig. 8 that the computed dorsal midline pressure shows good agreement with the experiment. The

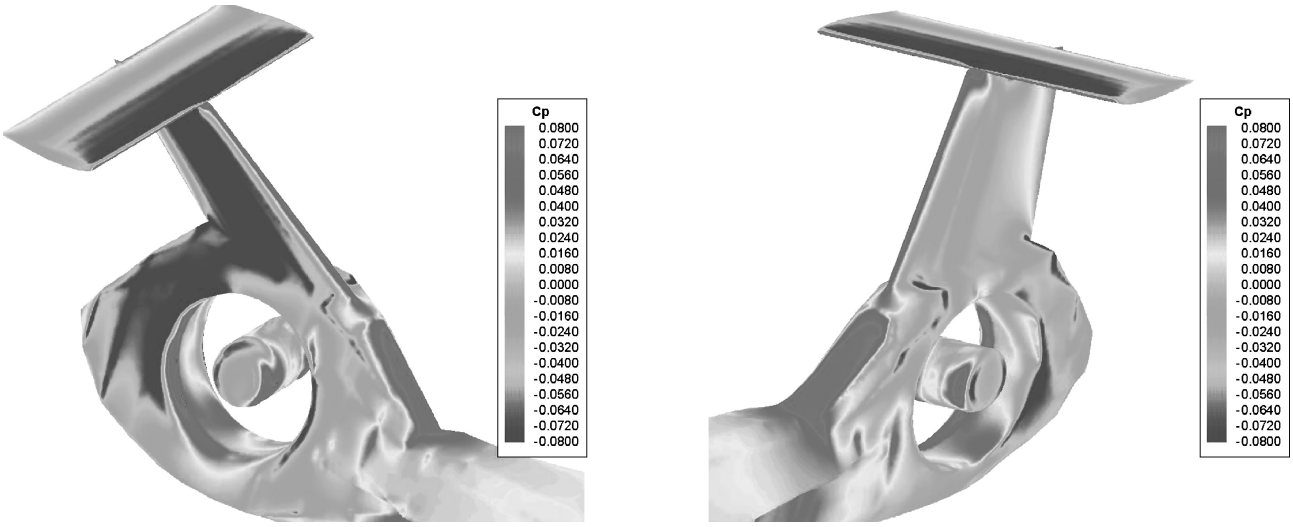

Fig. 15 ***Cp*** **contours in the vicinity of FANTAIL: forward flight, starboard and port views, with $V_\infty = 150$ kn and $\theta_{.75} = 0$ deg.**

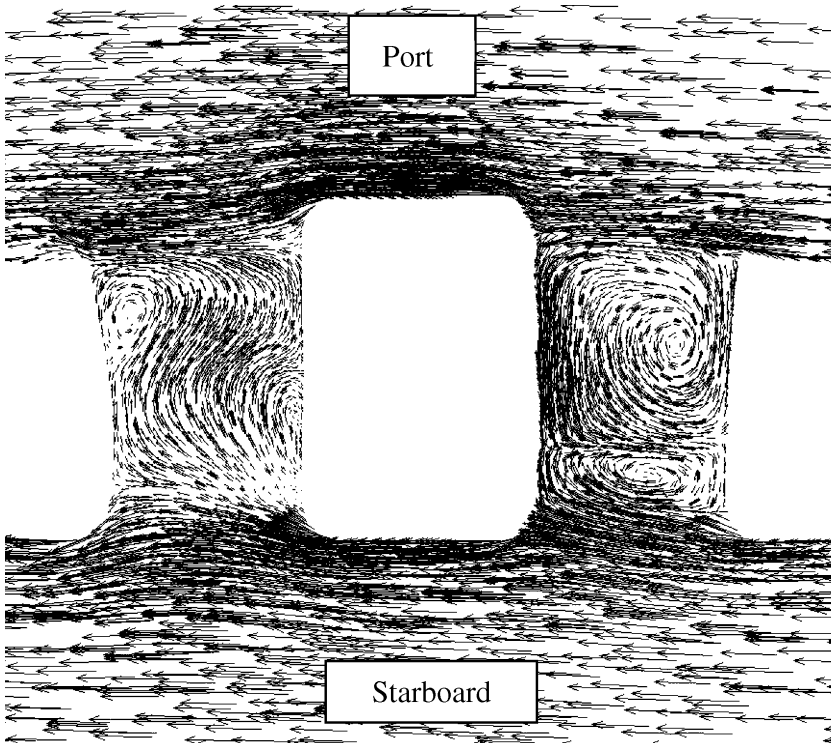

Fig. 16 Velocity vectors in the vicinity of FANTAIL: forward flight, with $V_\infty = 150$ kn and $\theta_{.75} = 0$ deg. (Net thrust is towards port side.)

slight discrepancies are most likely caused by slight geometric differences between the experimental and the computational model, the use of a uniform pressure jump assumption, and viscous effects.

Uniform-momentum theory might yield reliable results, but in reality the FANTAIL imposes a nonuniform pressure jump on the rotor disks.[12] In addition to this, uniform momentum theory cannot account for the pitch-angle settings of the blades. Therefore, as a more realistic approach, blade-element theory, which relates local pressure jump to local velocity field and blade pitch angle, is coupled with the CFD solution. Unlike the first method, where the fan thrust is given as input, in this case the blade pitch angle is specified, and the corresponding fan thrust is computed. Here the pitch angle is measured at the $\frac{3}{4}$-radius position.[3]

Figures 9–14 show pressure distributions and velocity vectors in the vicinity of the FANTAIL for pitch angles −10, 20, and 40 deg for the hover condition.

The effect of the blade pitch setting on the pressure distribution and the velocity field are evident in the figures. Also note from the figures that the suction of the fan creates a low-pressure region on the shroud around the inlet lip, which leads to additional antitorque moment.

Pressure and velocity distributions for the helicopter in forward flight with freestream velocity of 150 kn and collective pitch settings of 0, 20, and 40 deg are shown in Figs. 15–20.

In forward flight low fan thrust is desired to minimize drag and power consumption.[3] Figures 15, 17, and 19 clearly show that increasing the blade pitch angle creates a high-pressure region on the downstream side of the duct. This results in a significant aft force. To give better overall performance, it is desirable to design the vertical tail so that the fan is unloaded in trim. Note that this design approach also tends to push the fan into the region, near 0 deg of pitch, where the trim flow through the duct is not well defined as

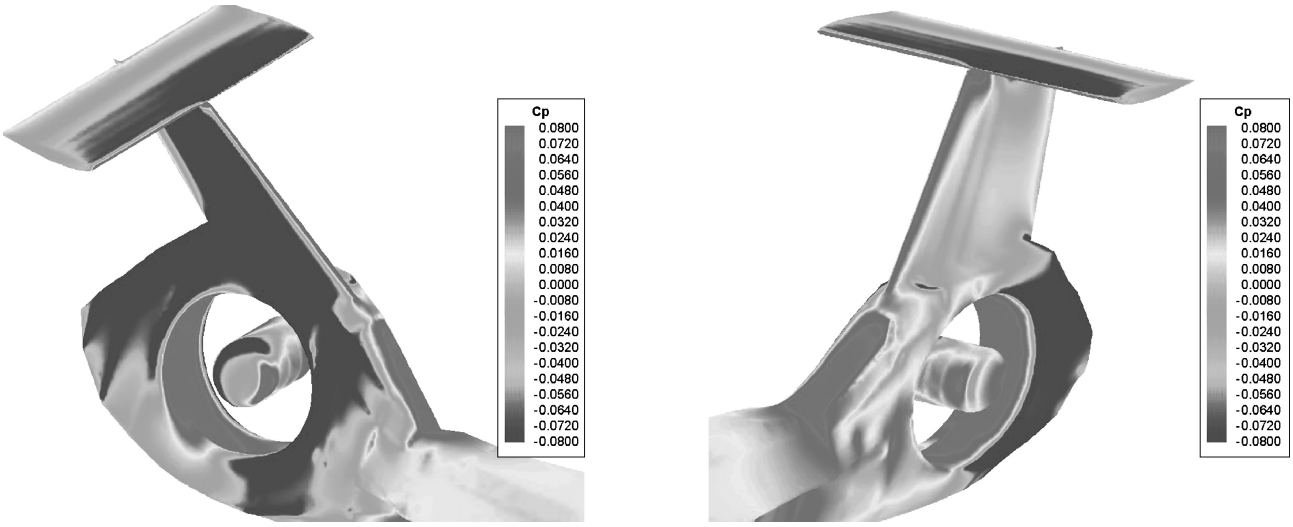

Fig. 17 ***Cp*** **contours in the vicinity of FANTAIL: forward flight, starboard and port views, with $V_\infty = 150$ kn and $\theta_{.75} = 20$ deg.**

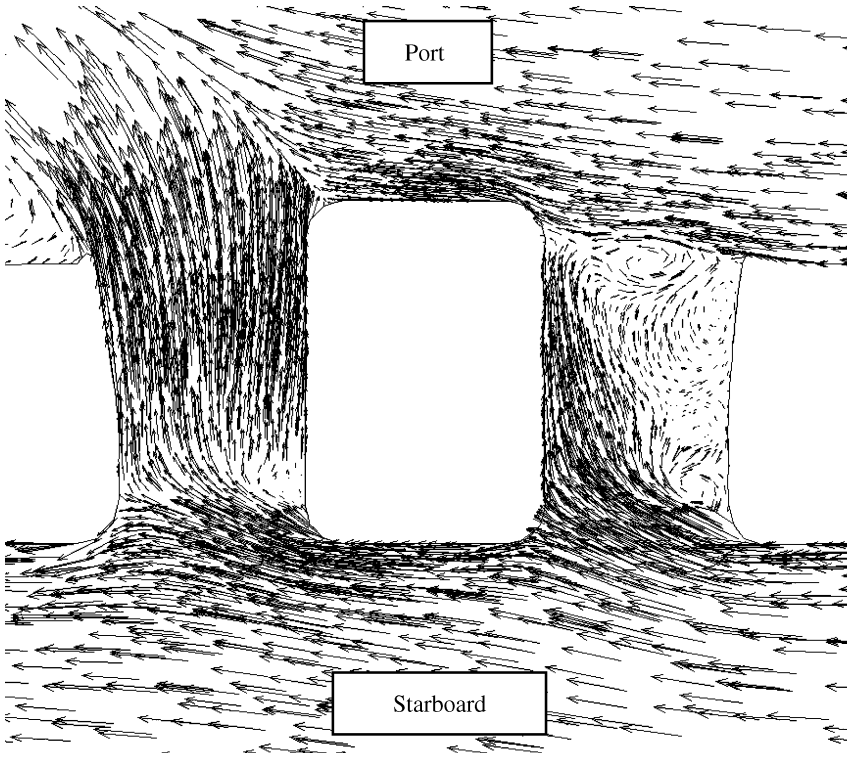

Fig. 18 Velocity vectors in the vicinity of FANTAIL: forward flight, with $V_\infty = 150$ kn and $\theta_{.75} = 20$ deg. (Net thrust is towards starboard side.)

can be seen from Fig. 16. In addition to this, a low pressure region develops on the port side of the shroud with increasing pitch angle. This also tends to decrease the total thrust. Unloading the fan also eliminates this effect.

Another important flight condition is sideward flight. Because the flow goes directly through the fan, the inflow velocities and consequently the local angle of attack of the blades change drastically. Figures 21 and 22 show the pressure and velocity distributions around the FANTAIL when the helicopter is in a left sideward flight of 45 kn and the collective pitch setting is 0 deg.

Figures 10, 12, 14, 16, 18, 20, and 22 show that except for the hover case with positive fan thrust the flow through the duct is not well defined. Separated flow regions can be easily seen in the vicinity of the duct and the centerbody. This also shows that the Euler equations are able to predict these kinds of flow when the separation is from a sharp edge and is Reynolds number independent. (For Reynolds-number-dependent flows one would have to use the Navier–Stokes equations.)

To analyze the control characteristics of the FANTAIL, thrust predictions are plotted as a function of the collective pitch angle for different flight conditions, and the results are compared with wind-tunnel data.[3,15,31] Here the total thrust generated by the FANTAIL and the thrust generated by the fan only are compared with the experiments separately. Figure 23 illustrates the relationship between the collective pitch angle and the total thrust in hover condition. Comparisons of the thrust generated by the fan only with the wind-tunnel data for hover and right sideward flight at a speed of 45 kn are available in Figs. 24 and 25. Solidity appearing in the figures is defined as

$$\sigma = \frac{N_b \cdot c \cdot (R - R_{\mathrm{cb}})}{\pi\left(R^2 - R_{\mathrm{cb}}^2\right)} = \frac{N_b \cdot c}{\pi(R + R_{\mathrm{cb}})} \tag{10}$$

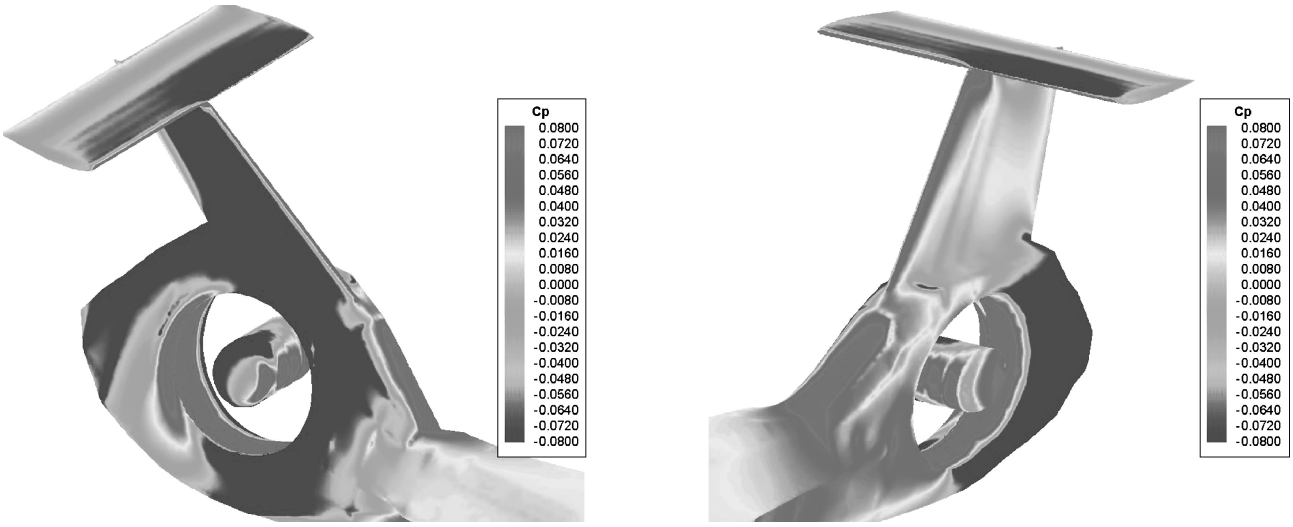

Fig. 19 ***Cp*** **contours in the vicinity of FANTAIL: forward flight, starboard and port views, with $V_\infty = 150$ kn and $\theta_{.75} = 40$ deg.**

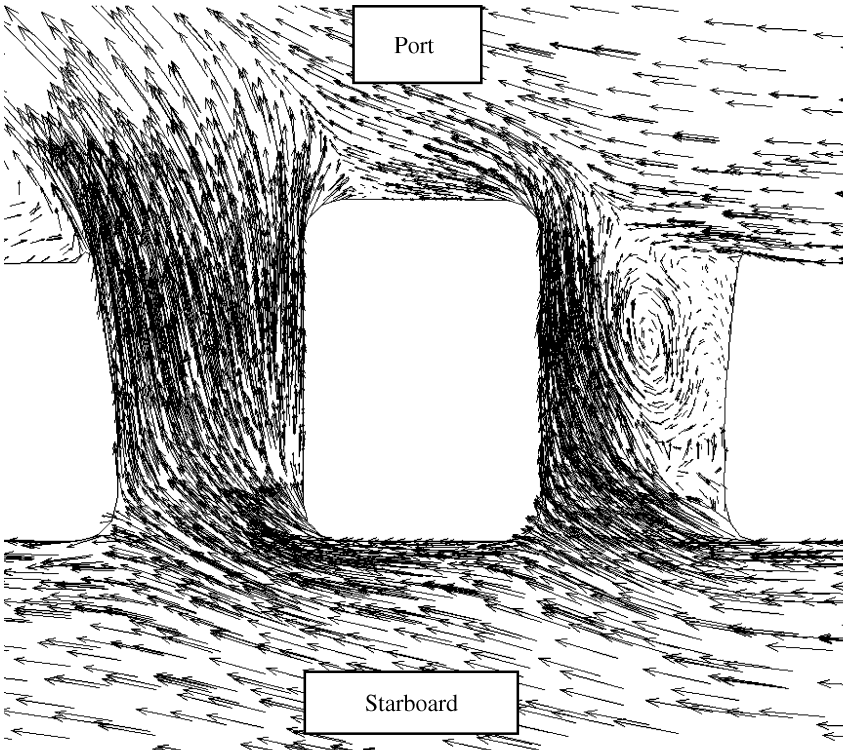

Fig. 20 Velocity vectors in the vicinity of FANTAIL: forward flight, with $V_\infty = 150$ kn and $\theta_{.75} = 40$ deg. (Net thrust is towards starboard side.)

Another result of interest from the static thrust results is that the ratio of total device thrust to fan thrust is about 1.83 and is very nearly independent of collective pitch. This value is very close to the ideal augmentation factor of 2.0.

The figures show that the results are generally in excellent agreement with the wind-tunnel data. The differences are most likely caused by the inviscid flow and linear lift-curve assumptions.

Figures 24 and 25 clearly showed that the fan thrust for a given collective pitch setting changes according to the flight condition of the aircraft. To display this effect in more detail, fan thrust is plotted as a function of pitch angle for hover, forward flight, and sideward flight in Fig. 26.

Results show that the introduction of forward speed causes a dramatic change in the thrust slope (change in thrust per degree of collective) near zero collective, a result that qualitatively agrees with flight data[5] and is critical for the setting of feedback gain schedule. Right sideward flight is analogous to a main rotor in a vertical climb where the freestream velocity adds to the inflow and decreases the local angle of attack of the blades. This results in less thrust for a given collective pitch setting than in hover. In left sideward flight this situation is reversed, and the fan acts like a rotor in vertical descent. The freestream velocity decreases the inflow and increases the local angle of attack of the blades. For low pitch angles the fan creates more thrust than in hover. But for high pitch settings this effectiveness will decrease because of the increasing induced flow.

Having the code validated, steady-state results can further be used to obtain basic directional stability characteristics of the helicopter. Weathercock stability, which is essentially the variation of yawing moment with sideslip angle, is one of them. Figure 27 shows the variation of aircraft yawing moment with sideslip angle in forward flight with 0 deg of collective pitch setting. The yawing moment presented in Fig. 27 is computed with respect to the nose of the

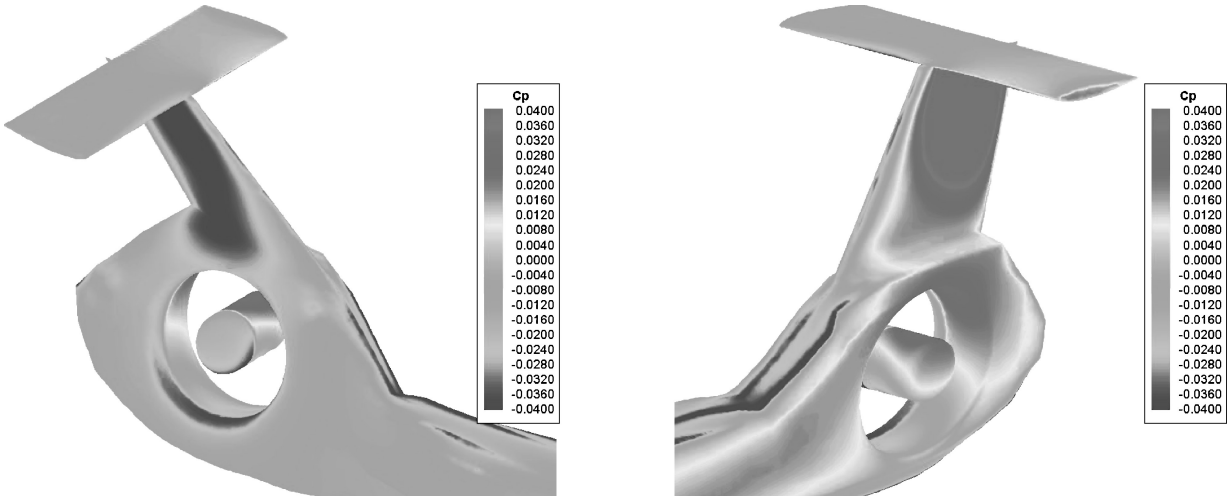

Fig. 21 ***Cp*** **contours in the vicinity of FANTAIL: left sideward flight, starboard and port views, with $V_\infty = 45$ kn and $\theta_{.75} = 0$ deg.**

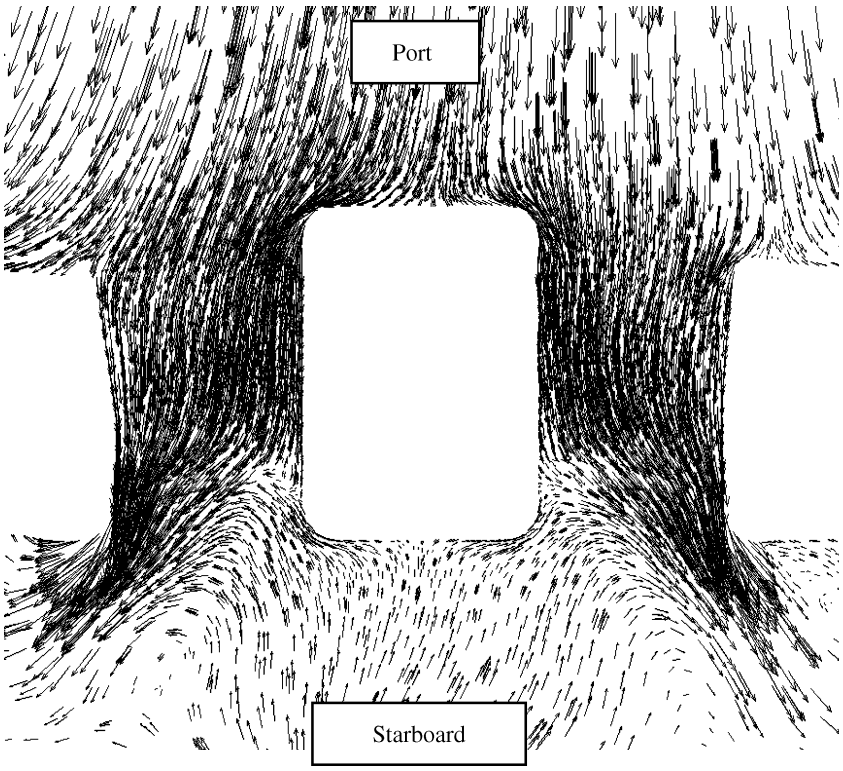

Fig. 22 Velocity vectors in the vicinity of FANTAIL: left sideward flight, with $V_\infty = 45$ kn and $\theta_{.75} = 0$ deg. (Net thrust is towards starboard side.)

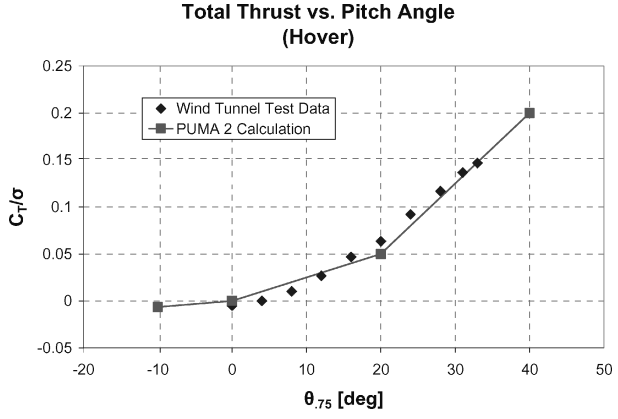

Fig. 23 Comparison of total thrust with experiment: hover.

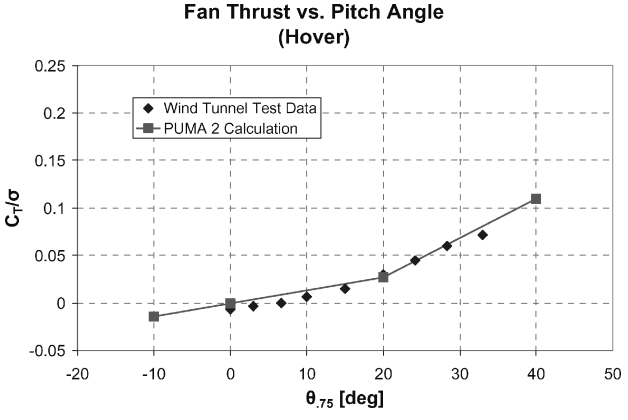

Fig. 24 Comparison of fan thrust with experiment: hover.

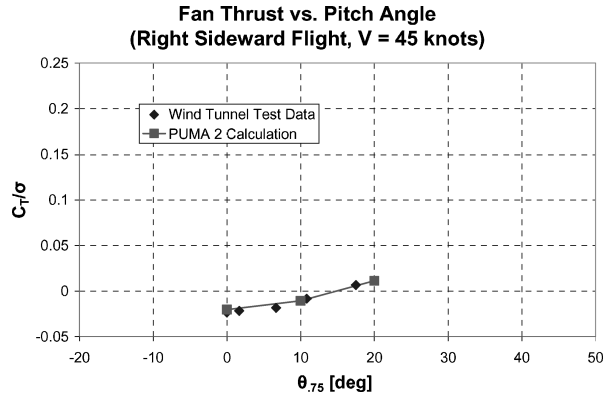

Fig. 25 Comparison of fan thrust with experiment: right sideward flight, with $V_\infty = 45$ kn.

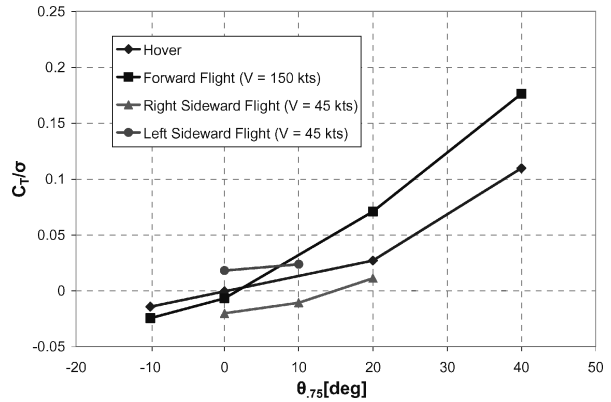

Fig. 26 Fan thrust characteristics in different flight conditions.

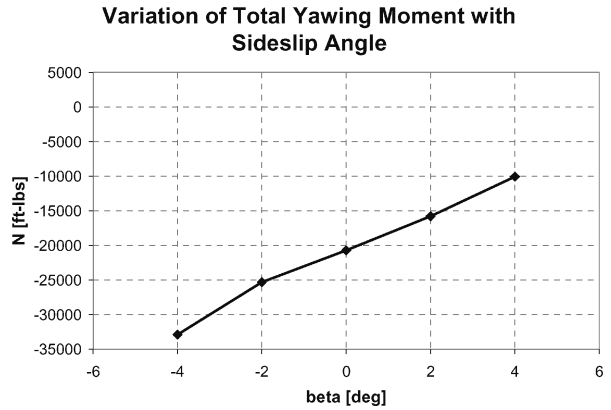

Fig. 27 Variation of yawing moment with sideslip angle: forward flight, with $V_\infty = 150$ kn and $\theta_{.75} = 0$ deg.

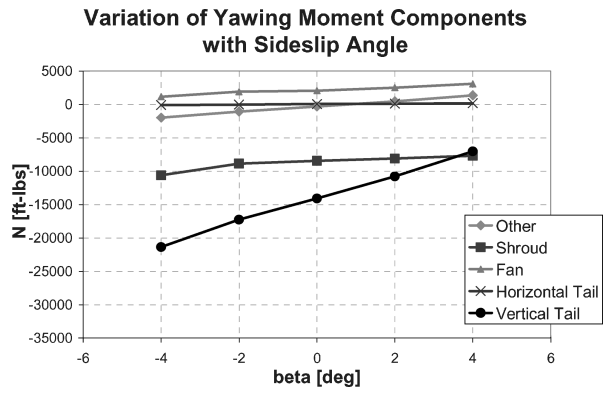

Fig. 28 Variation of yawing moment components with sideslip angle: forward flight, with $V_\infty = 150$ kn and $\theta_{.75} = 0$ deg.

aircraft. For stability the slope of the line must be positive. It is evident from the figure that the aircraft is stable in this sideslip angle range. These calculations were performed using inviscid flow assumption. It is known that viscous wake of the fuselage and flow separation occurring on the vertical tail at high sideslip angles lead to directional instabilities.

In forward flight the fuselage also generates a significant amount of antitorque moment. For a more detailed analysis variations of yawing moments generated by fan, shroud, horizontal tail, vertical tail, and other fuselage surfaces with sideslip angle are displayed in Fig. 28. As expected, the vertical tail is the dominant contributor of weathercock stability. The word "other" seen in the legend of the figure stands for all other fuselage surfaces except shroud, horizontal tail, and vertical tail.

Conclusions

Numerical simulations of flowfields around the RAH-66 Comanche helicopter were performed for various flight conditions with and without the FANTAIL operating. In the solutions the FANTAIL was modeled using an actuator disk and blade-element methods. The first method included the application of momentum theory, and the desired fan thrust was achieved by applying a uniform pressure jump across the rotor disk. The second method consisted of coupling blade-element theory with computational fluid dynamics, in which the fan thrust was computed as a function of collective pitch setting and local velocity field. Momentum theory results provided a preliminary knowledge of the effects of the FANTAIL on the overall flowfield. Blade-element theory allowed us to obtain a relationship between the fan thrust and collective pitch settings for different flight conditions. These relations were very important for the design and analysis of the flight-control system of the aircraft.

The computed results showed good agreement with the wind-tunnel data. The differences were most likely caused by geometric differences and the use of an inviscid solver, but the agreement was very good. It might also be beneficial to use more representative blade lift curves. In general, however, these were very encouraging results and show that computational fluid dynamics can be used to evaluate the static FANTAIL control effectiveness. Part II of these papers will explore the unsteady aerodynamic response to dynamic control inputs.

Acknowledgments

The flight testing described in this paper was conducted under the U.S. Army's RAH-66 Early Operational Capability Phase III Contract DAAJ09-91-C-A004. We would also like to acknowledge funding from the National Rotorcraft Technology Center (Grant NGT2-52275) for the Penn State Rotorcraft Center of Excellence. We would also like to thank the National Science Foundation for equipment grants (Grant Number NSF-EIA99-77526).

References

[1]Mouille, R., "The 'Fenestron' Shrouded Tail Rotor of the SA-341 Gazelle," *AHS Journal*, Vol. 15, No. 4, 1970, pp. 31–37.

[2]Mouille, R., "The 'Fenestron'—a Shrouded Tail Rotor Concept for Helicopters," *Proceedings of the AHS 42nd Annual Forum*, American Helicopter Society, Alexandria, VA, June 1986.

[3]Wright, G. P., Driscoll, J. T., and Nickerson, J. D., Jr., "Handling Qualities of the H-76 FANTAIL™ Demonstrator," *Proceedings of the AHS 47th Annual Forum*, American Helicopter Society, Alexandria, VA, May 1991.

[4]Lappos, N. D., and Phelps, K. D., "Results of Flight Tests of the Boeing-Sikorsky FANTAIL™ Demonstrator," *Proceedings of the AHS 47th Annual Forum*, American Helicopter Society, Alexandria, VA, May 1991.

[5]Kothmann, B. D., and Ingle, S. J., "RAH-66 Comanche Linear Aeroservoelastic Stability Analysis: Model Improvements and Flight Test Correlation," *Proceedings of the AHS 54th Annual Forum*, American Helicopter Society, Alexandria, VA, May 1998.

[6]Stiles, L., Armbrust, J., and Gaylor, C., "Comanche Tail Feathers—Code or Tin?," SETP Annual Meeting, 2001.

[7]Kothmann, B. D., and Armbrust, J., "RAH-66 Comanche Core AFCS Control Law Development: DEMVAL to EMD," *Proceedings of the AHS 58th Annual Forum*, American Helicopter Society, Alexandria, VA, May 2002.

[8]Jameson, A,. "Successes and Challenges in Computational Aerodynamics," AIAA Paper 87-1184, June 1987.

[9]Maskew, B., "Prediction of Subsonic Aerodynamic Characteristics—A Code for Low-Order Panel Methods," Paper AIAA 81-0252, 1981.

[10]Chaffin, M. S., and Berry, J. D., "Navier-Stokes and Potential Theory Solutions for a Helicopter Fuselage and Comparison with Experiment," ATCOM, Technical Rept. 94-A-013, June 1994.

[11]Lee, R. A., and Dash, S. M., "Helicopter Plume Flowfield Simulations for Signature Prediction in SPIRITS-HC," JANNAF, Feb. 1993.

[12]Duque, E. P. N., Berry, J. D., Budge, A. M., and Dimanlig, A. C. B., "A Comparison of Computed and Experimental Flowfields of the RAH-66 Helicopter," *Proceedings of the 1995 AHS Aeromechanics Specialists Meeting*, American Helicopter Society, Alexandria, VA, Oct. 1995.

[13]Duque, E. P. N., and Dimanlig, A. C. B., "Navier-Stokes Simulation of the AH-66 (Comanche) Helicopter," *Proceedings of the 1994 AHS Aeromechanics Specialists Meeting*, American Helicopter Society, Alexandria, VA, Jan. 1995.

[14]Costes, M., Collercandy, R., Kroll, N., von Geyr, H. F., Renzoni, P., Amato, P., Kokkalis, A., Rocchetto, A., Serr, C., Larrey, E., Filippone, A., and Wehr, D., "Navier-Stokes Calculations of Helicopter Fuselage Flowfield and Loads," *Proceedings of the AHS 54th Annual Forum*, American Helicopter Society, Alexandria, VA, May 1998.

[15]Rajagopalan, R. G., and Keys, C. N., "Detailed Aerodynamic Design of the RAH-66 FANTAIL™ Using CFD," *Proceedings of the AHS 49th Annual Forum*, American Helicopter Society, Alexandria, VA, May 1993.

[16]Leishman, J. G., *Principles of Helicopter Aerodynamics*, Cambridge Univ. Press, Caqmbridge, England, UK, 2000.

[17]Modi, A., Long, L. N., Sezer-Uzol, N., and Plassmann, P., "Scalable Computational Steering System for Visualization of Large-Scale CFD Simulations," AIAA Paper 2002-2750, June 2002.

[18]Souliez, F., Long, L., N., Morris, P. J., and Sharma, A., "Landing Gear Aerodynamic Noise Prediction Using Unstructured Grids," *International Journal of Aeroacoustics*, Vol. 1, No. 2, 2002.

[19]Modi, A., "Unsteady Separated Flow Simulations Using a Cluster of Work Stations," M.S. Thesis, Penn State Univ., Aerospace Engineering Dept., University Park, PA, May 1999.

[20]Souliez, F., "Parallel Methods for Computing Unsteady Separated Flows around Complex Geometries," Ph.D. Dissertation, Penn State Univ., Aerospace Engineering Dept., University Park, PA, Aug. 2002.

[21]Modi, A., and Long, L. N., "Unsteady Separated Flow Simulations Using a Cluster of Workstations," AIAA Paper 2000-0272, Jan. 2000.

[22]Modi, A., Long, L., and Plassmann, P., "Real-Time Visualization of Wake-Vortex Simulations using Computational Steering and Beowulf Clusters," VECPAR, Portugal, June 2002.

[23]Hansen, R. P., and Long, L. N., "Large Eddy Simulation of a Circular Cylinder on Unstructured Grids," AIAA Paper 2002-0982, Jan. 2002.

[24]Long, L. N., and Modi, A., "Turbulent Flow and Aeroacoustics Simulations Using a Clusters of Workstations," NCSA Linux Revolution Conf., June 2001.

[25]Sharma, A., and Long, L. N., "Airwake Simulations on an LPD 17 Ship," AIAA Paper 2001-2589, June 2001.

[26]Long, L. N., Souliez, F., and Sharma, A., "Aerodynamic Noise Prediction Using Parallel Methods on Unstructured Grids," AIAA Paper 2001-2196, May 2001.

[27]Souliez, F., and Long, L. N., "Computational Simulations of Rotorcraft Fuselage Drag," *Journal of the American Helicopter Society* (submitted for publication).

[28]Schweitzer, F., "Computational Simulation of Flow around Helicopter," M.S. Thesis, Penn State Univ., Aerospace Engineering Dept., University Park, PA, May 1999.

[29]Hansen, R., "Separated Turbulent Flow," Ph.D. Dissertation, Penn State Univ., Mechanical Engineering Dept., University Park, PA, Aug. 2001.

[30]Snir, M., Otto, S. W., Huss-Lederman, S., Walker, D. W., and Dongarra, J., *MPI, The Complete Reference*, MIT Press, Cambridge, MA, 1996.

[31]Keys, C., Sheffer, M., Weiner, S., and Heminway, R., "LH Wind Tunnel Testing: Key to Advanced Aerodynamic Design," *Proceedings of the AHS 47th Annual Forum*, American Helicopter Society, Alexandria, VA, May 1991.